Finding synaptic couplings from a biophysical model of motor evoked potentials after theta-burst transcranial magnetic stimulation

Marcus T. Wilson*[a], Mitchell R. Goldsworthy[b,c,d], Ann-Maree Vallence[e,f], Alex Fornito[g], Nigel C. Rogasch[d,g,h]

*Corresponding author: Te Aka Mātuatua–School of Science, University of Waikato, Private Bag 3105, Hamilton 3240, New Zealand; telephone +6478384834; fax +6478384835; email marcus.wilson@waikato.ac.nz

[a] Te Aka Mātuatua–School of Science, University of Waikato, Hamilton, New Zealand
[b] Lifespan Human Neurophysiology Group, Adelaide Medical School, University of Adelaide, Adelaide, Australia
[c] Hopwood Centre for Neurobiology, Lifelong Health Theme, South Australian Health and Medical Research Institute (SAHMRI), Adelaide, Australia
[d] Discipline of Psychiatry, Adelaide Medical School, University of Adelaide, Adelaide, Australia
[e] Discipline of Psychology, College of Science, Health, Engineering and Education, Murdoch University, Perth, Australia
[f] Centre for Healthy Ageing, Health Futures Institute, Murdoch University, Perth, Australia
[g] Turner Institute for Brain and Mental Health, School of Psychological Sciences, and Monash Biomedical Imaging, Monash University, Victoria, Australia
[h] South Australian Health and Medical Research Institute, Australia

Abstract

Objective: We aimed to use measured input-output (IO) data to identify the best fitting model for motor evoked potentials.

Methods: We analyzed existing IO data before and after intermittent and continuous theta-burst stimulation (iTBS & cTBS) from a small group of subjects (18 for each). We fitted individual synaptic couplings and sensitivity parameters using variations of a biophysical model. A best performing model was selected and analyzed.

Results: cTBS gives a broad reduction in MEPs for amplitudes larger than resting motor threshold (RMT). Close to threshold, iTBS gives strong potentiation. The model captures individual IO curves. There is no change to the population average synaptic weights post TBS but the change in excitatory-to-excitatory synaptic coupling is strongly correlated with the experimental post-TBS response relative to baseline.

Preprint submitted to Brain Research *Version 9, 18 October 2022*

Conclusions: The model describes population-averaged and individual IO curves, and their post-TBS change. Variation among individuals is accounted for with variation in synaptic couplings, and variation in sensitivity of neural response to stimulation.

Significance: The best fitting model could be applied more broadly and validation studies could elucidate underlying biophysical meaning of parameters.

Keywords:
Motor Evoked Potential, Transcranial Magnetic Stimulation, cortical plasticity, modeling, neural field theory, theta burst stimulation

---

1. Introduction

Transcranial Magnetic Stimulation (TMS) is now a commonly-used non-invasive form of brain stimulation (Hallett, 2007; Ziemann et al., 2008; Pascual-Leone et al., 2000; Lefaucheur et al., 2014). In addition to clinical applications, for example for treatment of major depression, TMS is increasingly used to study the human nervous system. A single pulse applied at sufficient intensity can give rise to a descending volley of activity (Hallett, 2007; Di Lazzaro et al., 2012) and ultimately to a measurable electrical response on the skin above the target muscle, known as a motor-evoked potential (MEP) (Hallett, 2000). MEPs are well-used in the study of the corticomotor system. They have been used to study changes in cortical excitability following repetitive TMS (rTMS), which may relate to plasticity changes in cortical circuits similar to long-term potentiation (LTP) and long-term depression (LTD) (Cooke and Bliss, 2006). It is often assumed, explicitly or implicitly, that changes in cortical response post-repetitive stimulation are a result of plastic changes in synaptic coupling strengths (Ziemann et al., 2008; Lenz et al., 2016; Barry et al., 2014; Wilson et al., 2014; Fung and Robinson, 2013; Wilson et al., 2018). However, the relationship between underlying microscale mechanisms and macroscopic measurements such as TMS-induced MEPs remains unclear (Matheson et al., 2016).

Biophysical models have provided a mathematical description, typically using equations, of many TMS processes and phenomena (Wilson et al., 2018). The primary aims of such models are 1. to elucidate the effects of the microscale processes on measurable outputs such as the electroencephalogram (Rogasch and Fitzgerald, 2013) or MEP; and 2. to make useful predictions about how a person or population group might respond to a particular intervention. They can include modelling of neurons at various levels of detail, for example large networks of neurons (Esser et al., 2005), small detailed networks of neurons (Traub et al., 2003; Rusu et al., 2014; Moezzi et al., 2017) and population-based descriptions of neural firing rates (Deco et al., 2008; Pinotsis et al., 2014).

Recently, Wilson et al. (2021) have developed a MEP model, drawing from the small network model of Moezzi et al. (2017) and the neural field model NFTsim (Sanz-Leon et al., 2017). This approach allows the prediction of input-output (IO) response curves for MEPs as a result of single-pulse TMS over the motor-cortex. The model has successfully reproduced the experimental effects of short-interval intracortical inhibition (SICI), interval intracortical facilitation (ICF), and long-interval intracortical inhibition (LICI) (Valls-Solé et al., 1992; Kujirai et al., 1993), and also the cortical silent period following a TMS pulse with voluntary contraction. The model has also

shown that variable results can be obtained for continuous and intermittent theta burst stimulation (cTBS and iTBS respectively) (Huang et al., 2005), depending on individual cases, in accordance with common experimental findings (Ozdemir et al., 2021). This model allows the fitting of parameters to measured IO curves, thus allowing parameters such as synaptic coupling strengths to be found for individual responses.

Recently, interest has grown in individualized treatment protocols — that is, protocols that have been tailored to a particular individual based upon measurements made on that individual (Klimesch et al., 2003; Bikson et al., 2012; Brownjohn et al., 2014; Wilson et al., 2018; Saturnino et al., 2019). For example, protocols using different theta-burst frequencies might be considered. Validated physical models might assist such a tailoring of approach — for example model parameters might be found for a baseline IO curve from which the effects of various treatment protocols could be calculated.

Experimental IO curves for different subjects have been measured by Goldsworthy et al. (2016) before and after application of iTBS or cTBS. In the current work, we fit the model of Wilson et al. (2021) to these experimental data and to explore variation in synaptic weights and excitation thresholds for individuals before and after iTBS or cTBS. Specifically, we aimed to be able to predict how an individual will respond following iTBS or cTBS, based on their baseline IO curve. Goldsworthy et al. (2016) recorded IO curves measured as MEP against stimulus intensity as a percentage of resting motor threshold (RMT) for different subjects (n=18) before and for three time periods (0–7 minutes, 15–22 minutes and 30–37 minutes) after iTBS or cTBS. In the case of cTBS, the experiment was repeated over three sessions (Vallence et al., 2015). We acknowledge that the number of subjects is now considered small for a study on cTBS and iTBS modulatory effects, due to the known high variability between subjects. However, it is sufficient to demonstrate the application of our methodology. The IO curves and their changes post-stimulation have been extensively detailed and statistically analyzed in Goldsworthy et al. (2016) and Vallence et al. (2015). However, for the purposes of clarity, we present the key findings below.

Figure 1 shows MEPs against TMS amplitude (measured as a percentage of RMT) for (a) iTBS and (b) cTBS, averaged over all subjects and time periods, and, for the case of cTBS, sessions. The baseline (dashed line) responses are slightly different for the iTBS and cTBS experiments of Goldsworthy et al. (2016) and Vallence et al. (2015) respectively. The data is also shown in a relative form in parts (c) and (d). Here we have calculated the ratio of the post-TBS response to the baseline response for each subject, and then averaged over all subjects. In order to show the full range of variability of the data, Fig. 2 shows the IO curves for each individual, in

addition to the mean response. From these plots it is clear that iTBS gives rise to a strong increase in MEPs at intensities close to threshold, but a weak decrease in MEPs for higher intensities. cTBS leads to a general but small reduction in MEP across all intensities.

The responses to iTBS were significantly higher than baseline for low amplitude stimulations (specifically 110% RMT), and the response to cTBS was significantly lower than baseline for the higher amplitude responses (140 – 180% RMT), as well as at 120%RMT. In particular, the response at 110% RMT was higher than baseline for iTBS, and lower for cTBS. It is also noteworthy that there was large variation in MEPs across subjects. In Fig. 1 the error bars denote the standard error in the mean; the full spread across subjects (as shown in Fig. 2) is much larger.

In the current manuscript, we consider two questions. First, what variation is present in the baseline data, and can this variation be described in a biophysical manner using the Wilson et al. (2021) model? Secondly, what biophysical changes occur post-TBS, and can the model be used to make inferences about how parameters might change after TBS; for example whether modulation of MEP response is due to a change in excitatory-to-excitatory synaptic coupling?

To investigate the first question, we fitted the model to individual baseline IO curves, allowing different combinations of parameters to vary. We assessed the goodness of fit using the Akaike Information Criterion, to correct for overfitting. We thus identifed that all three of our considered parameters were important to provide a good fit and describe variation across subjects: a scaling on the TMS input amplitude (equivalent to a variation in threshold and width of the TMS-to-excitatory coupling); the excitatory-to-excitatory synaptic coupling w_{ee}; and the excitatory-to-inhibitory synaptic coupling w_{ie}.

The second question is addressed in a similar way fitting parameters to the post-iTBS and -cTBS data allowing only certain combinations of parameters to vary. We demonstrated that reasonable relative responses are obtained by considering scaling of the threshold and width of the TMS-to-excitatory coupling, and the excitatory-to-excitatory coupling and the excitatory-to-inhibitory coupling. We found that changes in excitation (defined as $w_{ee,\mathrm{post}} - w_{ee,\mathrm{pre}}$) are correlated with an individual's experimentally-measured response to TBS. In other words the modeling is able to represent changes occuring to synaptic couplings on an individual basis.

We emphasize that in the following work we use a model of MEPs in order to fit existing experimental data by varying specific biophysical parameters. The goal is to identify a model that could be applied generally to TMS studies involving MEPs, and elucidate the neurophysiological meaning of the parameters within the model. Ultimately this modeling could help identify

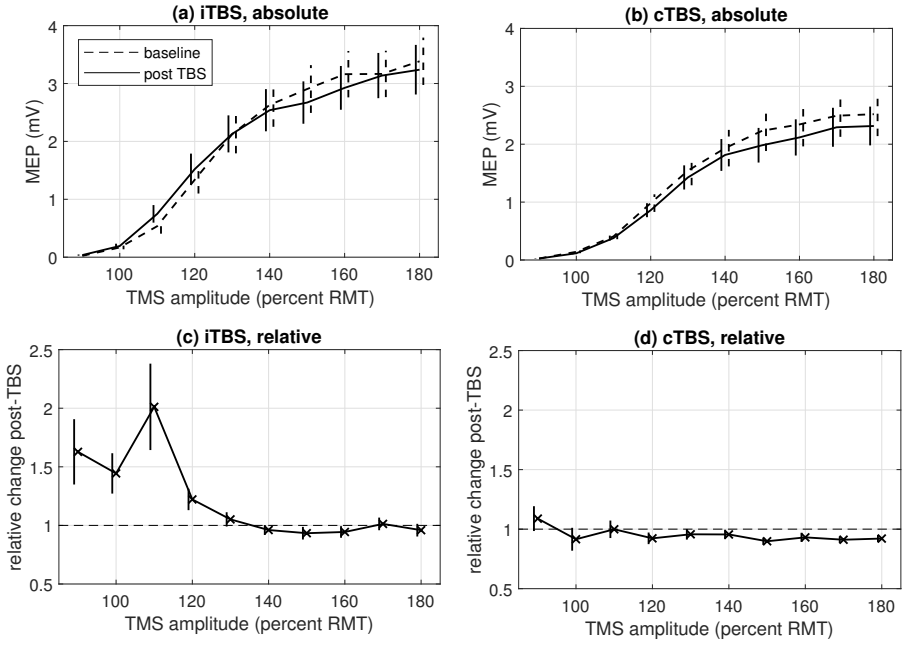

Figure 1: A plot of input-output and relative response curves for the data of Goldsworthy et al. (2016) and Vallence et al. (2015). (a) iTBS input-output. The mean baseline (dashed) and mean time-averaged MEP amplitude response following iTBS (solid) are plotted against input intensity (as a percentage RMT), averaged across all subjects. The vertical lines show the standard error in the mean across all subjects. (b) cTBS input-output. The mean baseline response (dashed) and mean time-averaged response following cTBS (solid) are plotted against input intensity (%RMT), averaged across all subjects and sessions. The vertical lines show the standard error in the mean across all subjects. (c) iTBS relative. The post-iTBS response is plotted as a fraction of the baseline response (i.e. the IO curve before iTBS stimulation). The bars are the standard error in the mean. (d) cTBS relative. The post-cTBS response is plotted as a fraction of the baseline response. The bars are the standard error in the mean.

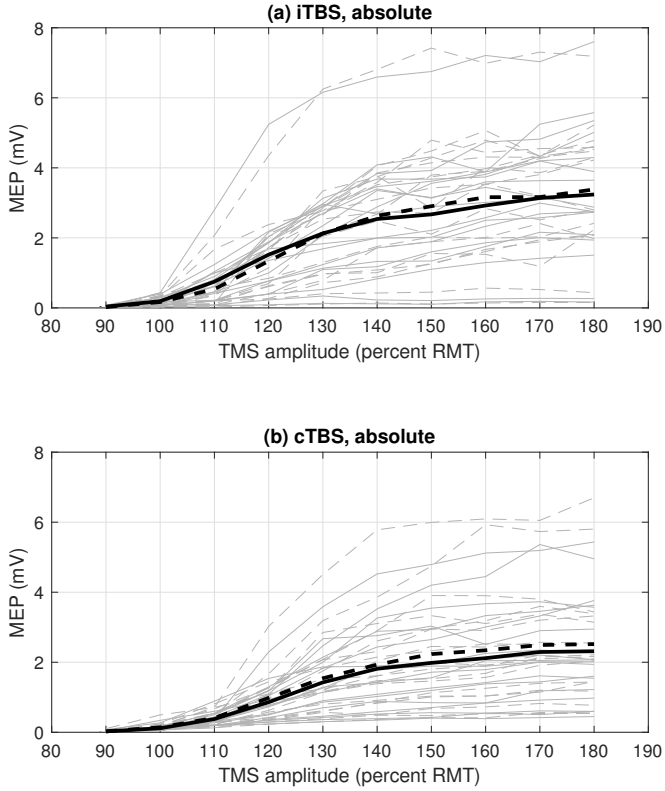

Figure 2: The IO curves for each individual for the case of (a) iTBS (dashed – pre, solid – post) and (b) cTBS (dashed – pre, solid – post). In both parts (a) and (b) the thick lines are the means across all individuals.

biophysical changes that might occur following interventions such as iTBS and cTBS.

2. Methods

2.1. Modeling of IO curves

The model is presented in full in Wilson et al. (2021), and summarized in Fig. 3(a). It consists of coupled populations of layer 2/3 excitatory neurons, layer 2/3 inhibitory neurons, and a population of layer 5 corticospinal output neurons. These feed motoneurons, whose firings result in motounit action potentials which are summed to create a MEP. Parameters, which are constrained to a lesser or greater extent by physical arguments (Robinson et al., 2004), have been optimized to fit experimental data (Fung and Robinson, 2013, 2014; Wilson et al., 2021). For this work the values for the large majority of the parameters are as presented in Wilson et al. (2021), but we have specifically looked at varying excitatory-to-excitatory and excitatory-to-inhibitory synaptic couplings, w_{ee} and w_{ie} respectively.

We also need to consider the interaction between the electric field induced by a TMS pulse and the neural populations in the cortex. We describe the interactions phenomenologically via three coupling strengths: ν_{ex}, the strength of interaction between the applied field and the excitatory population; ν_{ix}, the strength of interaction between the applied field and the inhibitory population; and ν_{vx}, the strength of interaction between the applied field and layer 5 population. Physically these couplings are proportional to the mean strengths of the excitatory or inhibitory post-synaptic potentials produced due to a stimulation event (Deco et al., 2008; Sanz-Leon et al., 2017). We use equations that achieve a preferential stimulation of excitatory neurons at high intensity, but a preferential stimulation of inhibitory neurons at low intensity (Ziemann et al., 1996; Ilic et al., 2002). The phenomenological description of the interaction accounts for many biophysical processes that lead to stimulation of cells under an applied field. Specifically, the coupling ν_{ix} is constant, whereas the coupling ν_{ex} is described through a sigmoidal function of stimulation intensity ϕ_x

$$\nu_{ex} = \frac{\nu_{ex}^{\max}}{e^{(A-\phi_x)/B+1}}, \tag{1}$$

where $\nu_{ex}^{\max}$ is the maximum coupling (at high intensities), A is the threshold of the sigmoid and B is its width. In this work we scale the effect of the TMS amplitude in this equation, in effect introducing a new parameter μ that scales together the threshold and width of the sigmoid:

$$\nu_{ex} = \frac{\nu_{ex}^{\max}}{e^{(\mu A-\phi_x)/\mu B+1}}. \tag{2}$$

This can be considered as scaling the take-off point and rate-of-take-off of the interaction between external stimulus and excitatory population.

The three parameters (w_{ee}, w_{ie} and μ) have been singled-out because (i) they significantly affect MEP amplitudes, as demonstrated by Wilson et al. (2021) who analyzed the effect of varying all parameters in the model; (ii) there is considerable literature that considers changes in synaptic couplings as a cause for changes in MEPs seen post-TBS (Thickbroom, 2007; Delvendahl et al., 2012; Lenz et al., 2016); and (iii) experimental data shows that different subjects require different stimulation amplitudes to produce the same response. In addition to the scaling of the interaction between the external stimulus and excitatory population, there is a commensurate scaling of the interaction between the external stimulus and the Layer 5 population, as described in Wilson et al. (2021), where the layer 5 population receives one tenth the input of the layer 2/3 excitatory neurons. The interactions that we vary in this work are indicated in Fig. 3(a) by the bold blue arrows. A summary of the method and analyses is given in Fig. 3(b).

The scaling of the interaction curve through the parameter μ does not model directly an explicit biophysical process. However, it does indirectly consider biophysical interactions that result in the coupling of electromagnetic field with cortical neurons. Moreover, recent analysis of MEPs by Goetz et al. (2019) has shown that the variation in input currents to cortical cells need be considered to account for the full range of variation in MEPs seen experimentally.

2.2. Fitting parameters to individual response curves

For each individual's baseline IO curves we have obtained the best fits to the experimental data by considering variation in w_{ee}, w_{ie} and μ. Specifically, we have looked at the following options, in which one, two or all three parameters are varied. 1. Varying solely μ, which we denote by 'S', for 'Scale'; 2. Varying solely w_{ee}, ('ee'); 3. Varying solely w_{ie}, ('ie'); 4. Varying μ and w_{ee}, ('S+ee'); 5. Varying μ and w_{ie}, ('S+ie'); 6. Varying w_{ee} and w_{ie}, ('ee+ie'); 7. Varying μ, w_{ee} and w_{ie}, ('S+ee+ie'). Numerical values for the other parameters described in Wilson et al. (2021) are the 'standard' values used in that reference. We have chosen to look specifically at the full range of these options rather than simply fitting S+ee+ie in order to ascertain what is the minimum fitting that we require in order to successfully represent the data.

To perform the fitting, we have generated a look-up table of modeled IO curves for the different w_{ee} and w_{ie} parameter combinations. This enables us to quickly calculate a goodness-of-fit value for each parameter combination, and select the best curve. Specifically, our look-up table has w_{ee} ranging from

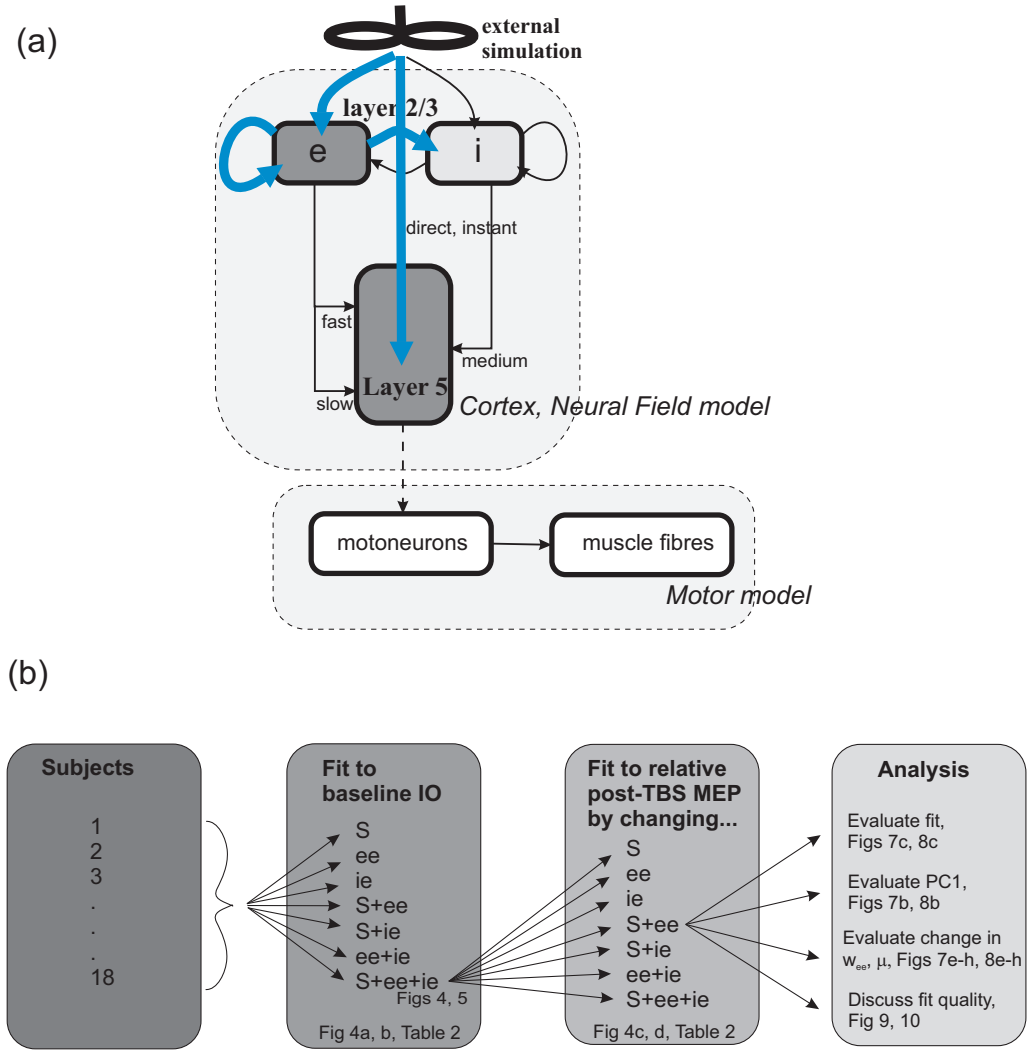

Figure 3: (a) A diagram of the interactions between the cellular populations of the model. The strength of the interactions shown with bold blue arrows are those that are modified in this work. Adapted from Wilson et al. (2021), Figure 1. e – excitatory neural population, i – inhibitory neural population.(b) A summary of the model analyses performed, and the figures where results are shown. S, ee and ie denote scaling of the parameters μ, w_{ee} and w_{ie} respectively, where w_{ee} is the excitatory-to-excitatory synaptic coupling strength, w_{ie} is the excitatory-to-inhibitory synaptic coupling strength, and μ controls the interaction between the external stimulus and excitatory population via Eq. (2).

0.75 to 1.05 times the standard value of 1.92×10^{-4} V s, in increments of 0.01 times its standard value; w_{ie} has the same range as w_{ee}. Since μ represents simply a scaling of the input amplitude (the x-axis) we only need look-up one curve for each w_{ee} and w_{ie} combination — then curves for various μ values from 0.5 to 2.0 in steps of 0.01 are quickly generated by interpolation. To describe the goodness of fit of a set of parameters, we use the Akaike Information Criterion (AIC) (Akaike, 1974) . The approach assesses relative quality of fitting of different models on a least-squares measure, but penalizes models with greater numbers of parameters. An alternative approach is provided by the Bayesian Information Criterion (BIC) which penalizes higher numbers of parameters more strongly than the AIC. Specifically, we construct a least-squares metric $\ln L$ as:

$$\ln L(\{p\}) = -\frac{1}{2} \sum_{j=1}^{18} \sum_{i=1}^{10} \frac{(m_{ij}(\{p\}) - \tilde{m}_{ij})^2}{\sigma_{ij}^2} \tag{3}$$

where $m_{ij}(\{p\})$ is the mean modeled MEP at the i-th intensity (90%, 100%, 110%, $\cdots$ 180%RMT) for the j-th person for the parameter set $\{p\}$, $\tilde{m}_{ij}$ is the mean measured MEP at the i-th intensity for the j-th person, and σ_{ij} is the standard error in the mean measured MEP at the i-th intensity for the j-th person. The weighted sum-of-squares deviation, χ^2, is simply $\chi^2 = -2\ln L$. The values of χ^2 should be interpreted in terms of the number of data points fitted. In Eq. (3) the sums are over 18 subjects and 10 intensities per subject, meaning χ^2 is a result of the fitting the model to 180 points. The AIC is then calculated as:

$$\mathrm{AIC} = 2k - 2\ln L, \tag{4}$$

where k is the number of fitted parameters. The value of k is 18, 36 or 54, for the cases of fitting one, two or three respectively of μ, w_{ee} and w_{ie} (being the number of parameters fitted per person times 18 people). Of importance is the difference between AIC for two different models; the lower score indicates that a model is more likely. We note that while we fit the model to each subject's IO curve individually, we assess the performance of the model across all subjects through a single value of χ^2 and AIC.

2.3. Changes in IO response post-TBS

We next assess how well the model captures changes in MEPs post-TBS. First, we consider the population as a whole; how well can the post-TBS changes be captured by the model? To do this, we look at responses relative to baseline across the different intensities since the relative response is how

such data are normally presented. For each individual j, we construct the relative measured IO response across TMS input intensities i, $\tilde{R}_j(i)$, as:

$$\tilde{R}_j(i) = \frac{\tilde{m}_{ij}^{\mathrm{TBS}}}{\tilde{m}_{ij}^{\mathrm{base}}}, \tag{5}$$

where $\tilde{m}_{ij}^{\mathrm{TBS}}$ is the measured MEP for person j at intensity i post-TBS, averaged across all time periods and sessions, and $\tilde{m}_{ij}^{\mathrm{base}}$ is the measured MEP for person j at intensity i at baseline, averaged across sessions. We have then fit the various combinations of the model parameters μ, w_{ee} and w_{ie} for each individual to best describe the *relative* response, as opposed to the IO curve itself. Thus the least-squares metric becomes:

$$\ln L(\{p\}) = -\frac{1}{2}\sum_{j=1}^{18}\sum_{i=1}^{10}\frac{\left(R_j(i) - \tilde{R}_j(i)\right)^2}{\Sigma_{ij}^2} \tag{6}$$

where $R_j(i)$ is the modeled relative response for the j-th individual at the i-th intensity, given by

$$R_j(i) = \frac{m_{ij}^{\mathrm{TBS}}}{m_{ij}^{\mathrm{base}}} \tag{7}$$

where m_{ij}^{TBS} is the modeled MEP for person j at intensity i post-TBS, averaged across all time periods and sessions, and m_{ij}^{base} is the modeled MEP for person j at intensity i at baseline, averaged across sessions. In Eq. (6) Σ_{ij}^2 is the standard error in the mean of the relative MEP at the i-th intensity for the j-th person.

Here we take m_{ij}^{base} as being the modeled MEP for the case of the S+ee+ie model since, as demonstrated in the results, this model provides the best overall fit to the baseline IO curves. When we fit the parameters to the post-TBS curves, we assess the model possibilities based on varying combinations of μ, w_{ee} and w_{ie}: S, ee, ie, S+ee, S+ie, ee+ie, and S+ee+ie. We emphasize that for post-TBS curves, we keep non-optimized parameters at their values that have resulted from the S+ee+ie fit to each individual's baseline IO curve. For example, for the 'ee' model, we fix μ and w_{ie} to be the values obtained after fitting S+ee+ie to the baseline IO curve, but allow w_{ee} to be further varied. This allows us to assess changes in parameters post-TBS compared to their pre-TBS values. For completeness, we also consider the model 'change nothing', that is, we do not vary μ, w_{ee} or w_{ie} from their baseline values. We do not expect this to give a good fit but it provides a control comparison for other models.

It is important to note that we have *fitted* model parameters to the post-TBS IO-curves. We have not *predicted* the post-TBS IO-curves using,

for example, calcium dependent plasticity equations implemented through NFTsim. This latter approach has been implemented in Fung and Robinson (2014) and Wilson et al. (2016, 2018). We are aiming to identify the best fitting model from the ones selected and more broadly to identify the biophysical role of the various parameters in controlling MEPs.

2.4. Principle Component Analysis to facilitate comparison between model and experiment

The first question we asked was "how well can the post-TBS changes be captured by the model?" The second question is "how well can changes for individual subjects be successfully reproduced?" That is, how well do modeled and measured MEPs align on an individual basis. For each individual j, we have ten data points (for the ten intensities 90% to 180% RMT) for $\tilde{R}_j(i)$ and $R_j(i)$. Comparison of the modeled and measured data for an individual involves consideration of these ten intensity values. Rather than working with ten values, we reduce the $\tilde{R}_j(i)$ and $R_j(i)$ responses to a single value using principal component analysis (PCA). We first find the ten principal components of the data $\tilde{R}_j(i)$. We then express, for each person j, their measured and modeled responses in terms of these principal components and extract the coefficient of the first, most significant, principal component, which we denote $\tilde{P}_j$ and P_j for the measured and modeled cases respectively. Thus we reduce the relative change in MEP across all intensities (i.e. the individual response curves making up Fig. 1(c) and (d) to a single-valued measure.) We then correlate P_j with $\tilde{P}_j$ to ascertain how well the model fitting deals with individual as opposed to populations of responses. Finally, we correlate changes in w_{ee}, w_{ie} and μ with $\tilde{P}_j$ to look at how changes in MEP relate to a change in parameters, for each individual j.

A summary of the method and analyses is given in Fig. 3(b). A table of the parameters used in this study, their meanings and range of values, is given in Table 1.

2.5. Code availability

The code to implement this study has been written in Matlab and is available at `https://github.com/mtwilson1970/Fitting_weights_to_meps`. The code draws from a look-up table which was created by running the MEP model described in Wilson et al. (2021), available at `https://github.com/mtwilson1970/MEP_modeling_2020`. The MEP model itself draws from the NFTsim model for modeling neural field equations; NFTsim is available at `https://github.com/BrainDynamicsUSYD/nftsim` (version 1.1.0) (Sanz-Leon et al., 2017).

Table 1: The model parameters and their values, and other symbols used in this manuscript.

	Description	Value or Range	Unit
	Model parameters (from Wilson et al. (2021))		
ν_{ex}^{max}	Maximum coupling between external field and excitatory population	1.92×10^{-4}	V s
ν_{ex}	Coupling between external field and excitatory population	As in Eq. (2)	V s
ν_{ix}	Coupling between external field inhibitory population	-1.92×10^{-4}	V s
ν_{vx}	Coupling between external field layer 5 population	$0.1\nu_{ex}$	V s
A	Threshold of field-to-excitatory coupling curve	500	s^{-1}
B	Width of field-to-excitatory coupling curve	100	s^{-1}
ϕ_x	Stimulation intensity	400 – 1600	s^{-1}
	Model parameters (fitted)		
μ	Scaling of threshold and amplitude of coupling	0.5 – 2	—
w_{ee}	Excitatory-to-excitatory coupling	$(0.75 – 1.05)\times 1.92 \times 10^{-4}$	V s
w_{ie}	Excitatory-to-inhibitory coupling	$(0.75 – 1.05)\times 1.92 \times 10^{-4}$	V s
	Experimental data descriptors		
$\tilde{m}_{ij}^{\text{base}}$	Mean measured MEP at i-th intensity for j-th person pre-TBS	See results	V
$\tilde{m}_{ij}^{\text{TBS}}$	Mean measured MEP at i-th intensity for j-th person post-TBS	See results	V
m_{ij}^{base}	Mean modeled MEP at i-th intensity for j-th person pre-TBS	See results	V
m_{ij}^{TBS}	Mean modeled MEP at i-th intensity for j-th person post-TBS	See results	V
$\tilde{R}_j(i)$	Relative measured IO response at i-th intensity for j-th person	See results	—
$R_j(i)$	Relative modeled IO response at i-th intensity for j-th person	See results	—
σ_{ij}	Standard error in mean measured MEP i-th person, j-th intensity	See results	V
Σ_{ij}	Standard error in measured relative MEP i-th person, j-th intensity	See results	V
	Analysis parameters		
k	Total number of fitted parameters	0, 18, 36, 54	—
χ^2	Weighted-sum-of-squares measure	As in Tab. 2	—
AIC	Akaike Information Criterion	As in Tab. 2	—

Table 2: Values of AIC and χ^2 for different models fitted to the baseline IO curves and the post-TBS relative response curves. Each model has been fitted to 180 data points (18 subjects times 10 intensities). k gives the total number of parameters fitted (number of parameters per subject, times 18 subjects). S – Scaling of input axis; ee – fitting only w_{ee}; ie – fitting only w_{ie}; ee+ie – fitting w_{ee} and w_{ie}; S+ee – Scaling of input axis and fitting w_{ee} synaptic couplings; S+ie – Scaling of input axis and fitting of w_{ie} synaptic coupling; S+ee+ie – Scaling of input axis and fitting of both w_{ee} and w_{ie} synaptic couplings.

		iTBS				cTBS			
		baseline		post-i		baseline		post-c	
Model	k	χ^2	AIC	χ^2	AIC	χ^2	AIC	χ^2	AIC
nothing	0	718	718	236	236	2043	2043	341	341
S	18	198	234	181	217	423	459	226	262
ee	18	358	394	184	220	768	804	216	252
ie	18	331	367	172	208	659	695	228	264
ee+ie	36	213	285	160	232	341	413	191	263
S+ee	36	66	138	122	194	140	212	168	240
S+ie	36	66	138	117	189	127	199	185	257
S+ee+ie	54	27	135	104	212	58	166	155	263

3. Results

3.1. Fitting parameters to baseline input-output curves

In Table 2 for iTBS and cTBS we show the AIC and χ^2 scores, along with values of k, for the different sets of parameters fitted. We also show AIC scores in graphical form in Fig. 4. The χ^2 values obtained for baseline fits are substantially lower (around half) for the S+ee+ie model than for any other model. The lowest AIC scores obtained for the baseline iTBS curves are for the S+ee, S+ie and S+ee+ie models, which all are similar and significantly lower than other models. For the baseline cTBS curves, these three are again lower than other possibilities, with the S+ee+ie model being lowest. In all cases, adding the 'S' option into the model improves the fit. E.g. the S+ee model outperforms the ee model; the S+ie model outperforms the ie model; the S+ee+ie model outperforms the ee+ie model. We conclude that the coupling between the amplitude of the stimulation and the neural response, modulated through the parameter μ in Eq. (2), is a key consideration in modeling of MEPs (Capaday, 2021). This is also suggested experimentally by Tang et al. (2016). The low scores for the S+ee+ie model justifies the choice of using this model to fit the baseline data prior to fitting post-TBS, Section 2.3.

Example fits to individuals are shown in Fig. 5. Here we show the fitted IO curves for all subjects for the baseline cTBS experiments, for the case of

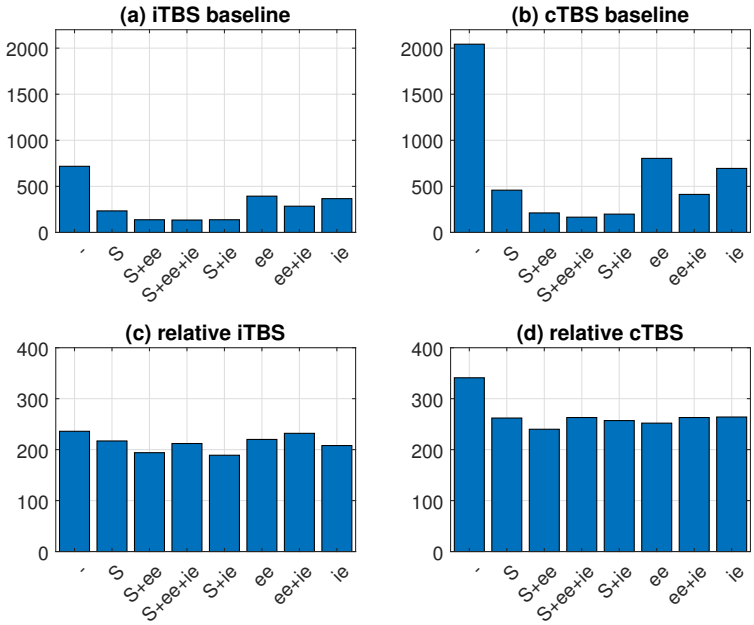

Figure 4: The AIC scores for (a) fitting to the pre-iTBS baseline IO curve; (b) fitting to the pre-cTBS baseline IO curve; (c) fitting to the post-iTBS relative MEP curve; (d) fitting to the post-cTBS relative MEP curve. Lower values show that a model is more likely. The symbol '–' denotes the 'change nothing' model.

scaling the input (i.e. allowing μ to vary), and fitting w_{ee} and w_{ie}. While the model fits well in most cases, there are some occasions (*e.g.* person 6) for which it does not.

Figure 6 gives fitted input-output curves for the case of person 6, for the baseline cTBS data. This example has been chosen because when either w_{ee} alone (pink dot-dash curve) or w_{ee} and w_{ie} together (thin pink-dash curve) are fitted, the model shows a particularly poor fit to the measured data. Specifically, this particular subject shows a very rapid increase in MEP with changing amplitude above 110% RMT, and a falling MEP at the highest amplitudes, which the model is unable to reproduce with scaling of synaptic couplings w_{ee} and w_{ie} alone. Fitting purely w_{ee}, shown by the pink dot-dash line, produces a fitted curve that vastly overestimates the MEP at low amplitudes. Fitting both w_{ee} and w_{ie}, shown by the thin pink-dash line, gives only a marginal improvement; the model now underestimates MEPs at mid-range amplitudes. Scaling of the input is additionally required (thick pink-dash) in order for the model to reasonably fit the data (although the fit is still poor). Capaday (2021) has analyzed the variance in MEP against MEP intensity. Variation in MEP intensity is largest near threshold and accurate modeling of the MEP is highly dependent on accurate identification of the threshold. In terms of our work, scaling of the input intensity directly addresses where the threshold of the sigmoid in Eq. (2) arises, without altering the MEP at very high or low stimulation amplitudes.

3.2. Fitting to post-TBS curves

We now discuss the fitting of the model to the post-iTBS and -cTBS IO curves. We start by considering the model fits across the population, and then look specifically at how well the model describes the responses of individuals.

3.2.1. Responses across the population

We first describe the fitting of the model to the population as a whole. In Table 2 and Fig. 4(c) and (d) for iTBS and cTBS respectively we give the AIC values resulting from fitting the model to all 18 individual time-averaged and session-averaged post-TBS response curves. For the iTBS case, the best performing models are S+ee and S+ie, with AIC scores of 194 and 189 respectively. These are lower than the next best performing models. For the cTBS case, the S+ee model is the lowest scoring, with an AIC of 240, although S+ie is close with a score of 257. Overall, variation in μ, that is, an 'S' part of the model, appears to be necessary post-TBS in order to fit the relative MEP data. In addition, varying w_{ee} or w_{ie}, i.e. a synaptic coupling term, improves the fit. However, on this basis we cannot definitively

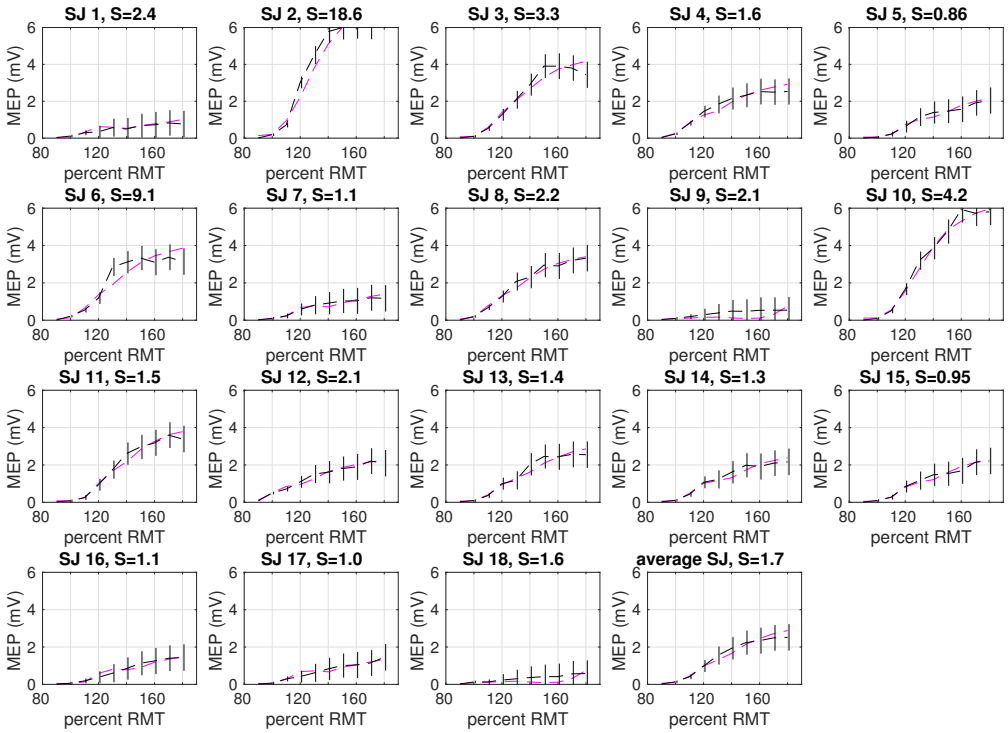

Figure 5: The fitted IO curves for all subjects (denoted 'SJ' for 'subject') for the case of the baseline of the cTBS experiment. In each subplot, black dashed line shows the measured MEP response, with the vertical black bars denoting the standard error in the mean. The fitted line (pink dash) is the output of the model when w_{ee}, $w_{ie}$and μ have been fitted. The value of the sum-of-squares deviation, $S_j = \sum_{i=1}^{10} \left(m_{ij} - \tilde{m}_{ij}\right)^2 / \sigma_{ij}^2$, is also shown, where m_{ij} is the modeled MEP at the i-th intensity for the j-th person, $\tilde{m}_{ij}$ is the measured MEP at the i-th intensity for the j-th person, and σ_{ij} is the standard error in the mean of the MEP at the i-th intensity for the j-th person. The final plot 'average pn' is the model fit to the data averaged over all subjects.

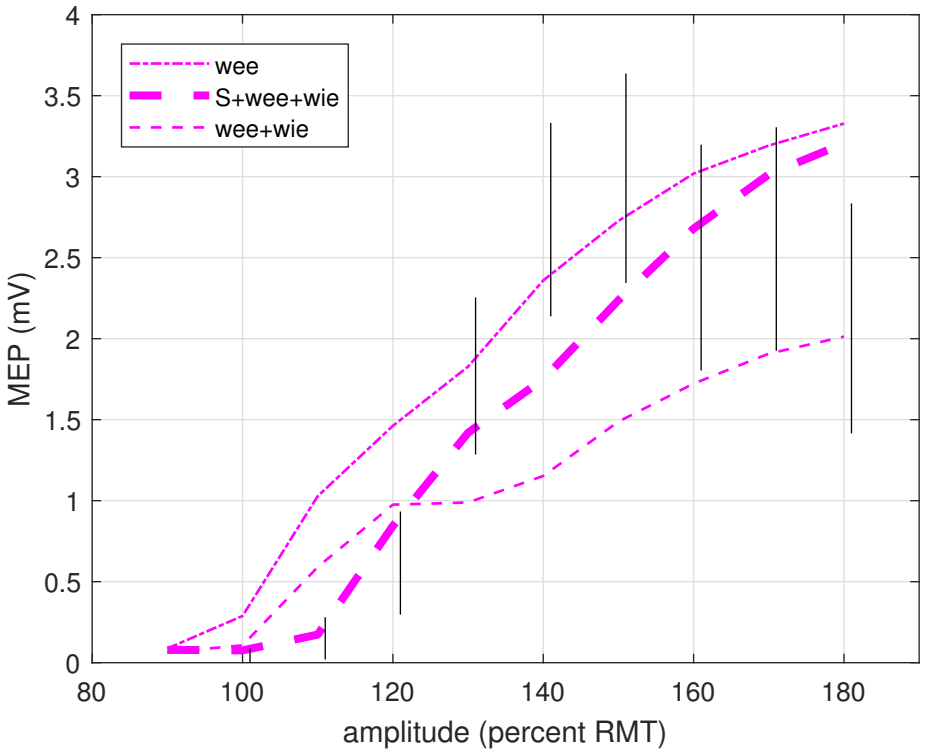

Figure 6: An example of the fit of the model to an individual's input-output curve (person 6, baseline for cTBS experiments) that shows an unusually rapid take-off in response post RMT. Vertical black bars show the measured pre-TBS data, as mean ± standard error in the mean, for a given amplitude (%RMT). The dot-dashed, dashed and thick-dashed lines show the model's fit to the experimental data for the cases of fitting w_{ee}, w_{ee} & w_{ie}, and w_{ee}, w_{ie} & input scaling respectively.

distinguish between the fitting of w_{ee} or w_{ie}. In other words the results do not allow us to conclude that, for example, w_{ee} changes in preference to w_{ie}, as has often been assumed in modeling work (Wilson et al., 2014; Sorkhabi et al., 2021; Fung et al., 2013; Fung and Robinson, 2013). Since the favored post-TBS models are S+ee and S+ie for iTBS, and S+ee for cTBS, we have concentrated on the S+ee model for post-TBS analysis in what follows.

Results are shown graphically in Figs. 7 and 8, for the case of iTBS and cTBS respectively. Here we show fits to the baseline IO curves using the S+ee+ie model, and the fits to the post-TBS relative MEP curves using the S+ee model. In these plots, we have used black to represent experimental data, pink to represent modeled data, a dashed line to represent pre-TBS data and a solid line to represent post-TBS data. Figure 7(a) shows the *measured* MEP data as bars (mean±s.e.m. across all subjects) for the pre-iTBS (black dashed) and post-iTBS (black solid) cases. The smooth pink lines show the mean across the population of the *modeled* results both pre-iTBS (pink dashed) and post-iTBS (pink solid) stimulation. Values of R^2 are indicated for fitting of the pre-iTBS and post-iTBS curves, where

$$R^2 = 1 - \frac{\sum_i (y_i - f_i)^2}{\sum_i (y_i - \bar{y})^2}, \tag{8}$$

where y_i is the mean experimentally-measured MEP at the i-th intensity, $\bar{y}$ is the mean of y_i across intensities and f_i is the mean fitted MEP at the i-th intensity. Part (c) shows the experimental and modeled data in terms of *relative* change, i.e. the experimental $\tilde{R}_j(i)$ averaged over all people j (mean±s.e.m., black) and the modeled $R_j(i)$ averaged over all people j (mean±s.e.m., pink). Figure 8(a) and (c) show the similar result for the cTBS case.

Figures 9 and 10 show histograms of the residual MEPs after fitting with the S+ee model (baseline) and S+ee+ie (post-TBS) model for the cases of iTBS and cTBS respectively. The plots show the cases for two stimulation intensities, 110%RMT and 180%RMT. These two intensities have been chosen because the 110%RMT case is where a significant potentiation effect is seen in the relative MEP for iTBS, and 180%RMT represents the maximum intensity used. The histograms have been tested for normality (Anderson-Darling test), zero mean (unpaired t-test) and skewness (Trujillo-Ortiz and Hernandez-Walls, 2003). Where the Anderson-Darling test for normality shows a p-value of less than 0.05, the test of whether the mean of the population is zero (t-test) is dubious. Results are shown in Tab. 3. It is evident that, for iTBS, the null hypothesis of a normal distribution cannot be discounted. For 110% RMT, both for baseline and post-iTBS, the residuals the population shows a mean that is statistically less than zero, that is the

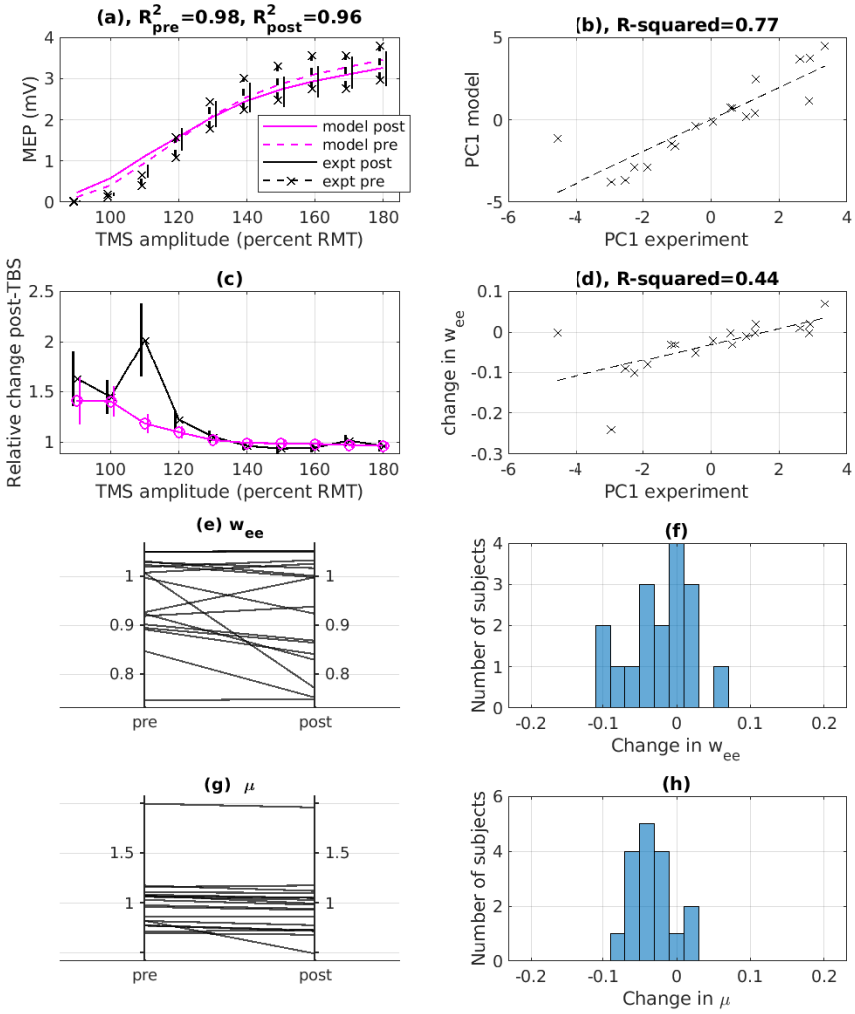

Figure 7: Measured data, and modeled fits, for iTBS. (a) Experimental IO data (dashed black bar, pre-iTBS, mean±s.e.m.; solid black bar, post-iTBS, mean±s.e.m.) and the population mean of the model fits to the pre-iTBS IO curve with the S+ee+ie model (pink dash) and the post-iTBS relative MEP curve with the S+ee model (pink solid). (b) The first principal component of the modeled relative response curve P_j, against the first principal component of the experimental relative response curve $\tilde{P}_j$, for all individuals j. (c) The relative change in MEP post-stimulation for the various intensities for the experimental data (black cross, mean±s.e.m) and the modeled fits (pink circle, mean±s.e.m.). (d) The change in modeled excitatory weight w_{ee} after iTBS, against the first principal component of the experimental relative response curve $\tilde{P}_j$, for all individuals j. (e) The pre- and post-iTBS values for w_{ee} for all individuals. (f) The distribution of the change in synaptic couplings w_{ee} across all individuals.(g) The pre- and post-iTBS values for μ for all individuals. (h) The distribution of the change in μ across all individuals.

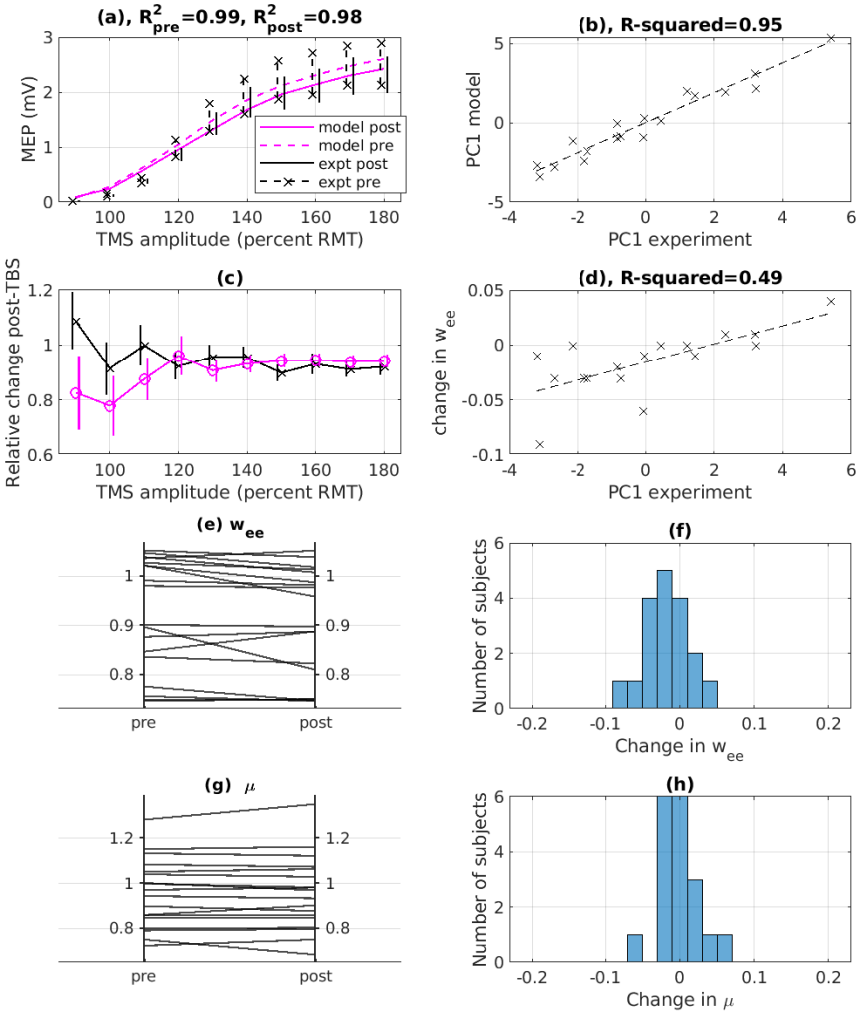

Figure 8: Measured data, and modeled fits, for cTBS. (a) Experimental IO data (dashed black bar, pre-cTBS, mean±s.e.m.; solid black bar, post-cTBS, mean±s.e.m.) and the population mean of the model fits to the pre-cTBS IO curve with the S+ee+ie model (pink dash) and the post-cTBS relative MEP curve with the S+ee model (pink solid). (b) The first principal component of the modeled relative response curve P_j, against the first principal component of the experimental relative response curve $\tilde{P}_j$, for all individuals j. (c) The relative change in MEP post-stimulation for the various intensities for the experimental data (black cross, mean±s.e.m) and the modeled fits (pink circle, mean±s.e.m.). (d) The change in modeled excitatory weight w_{ee} after cTBS, against the first principal component of the experimental relative response curve $\tilde{P}_j$, for all individuals j. (e) The pre- and post-cTBS values for w_{ee} for all individuals. (f) The distribution of the change in synaptic couplings w_{ee} across all individuals. (g) The pre- and post-iTBS values for μ for all individuals. (h) The distribution of the change in μ across all individuals.

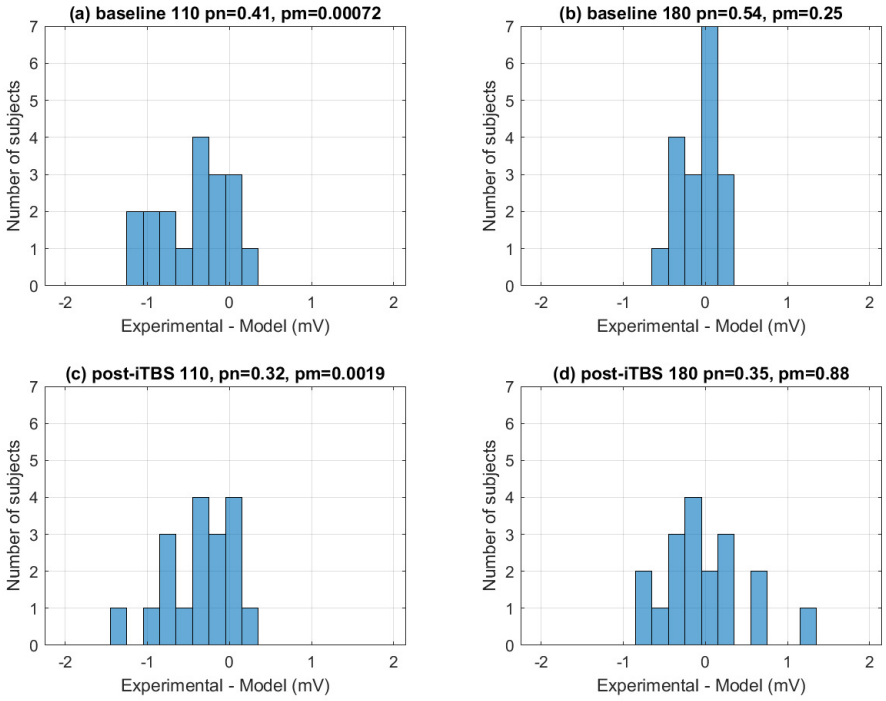

Figure 9: Histograms of the residual MEPs (in millivolts), defined as the experimental MEP minus the modeled MEP, for the iTBS experiments and modeling. (a) Baseline (pre-iTBS), 110% RMT. (b) Baseline, 180% RMT. (c) Post-iTBS, 110%RMT. (d) Post-iTBS, 180% RMT. The p-values for tests of normality (pn) and zero-mean (pm) are shown.

model overpredicts the MEP. For cTBS, the null hypothesis of a normal distribution can be discounted for the case of the baseline measurements at 180% RMT. For all cases the model shows a mean statistically lower than the experimental measurements, although not by as much as for the iTBS cases.

3.3. Responses for individuals

We now consider individual responses. Figure 7 parts (b) and (d) show this in detail for iTBS stimulation modeled with S+ee. Part (b) shows the correlation between measured and modeled first principal components, $\tilde{P}_j$ and P_j respectively, for all individuals j, as described in section 2.4. The data show significant correlation, indicating that, broadly speaking, the model can reproduce relative response curves on an individual basis. Part (d) shows how the change in excitation, defined as $(w_{ee,j})_{\text{post}} - (w_{ee,j})_{\text{pre}}$, correlates with the experimental relative response $\tilde{P}_j$ for all individuals j. A positive correlation

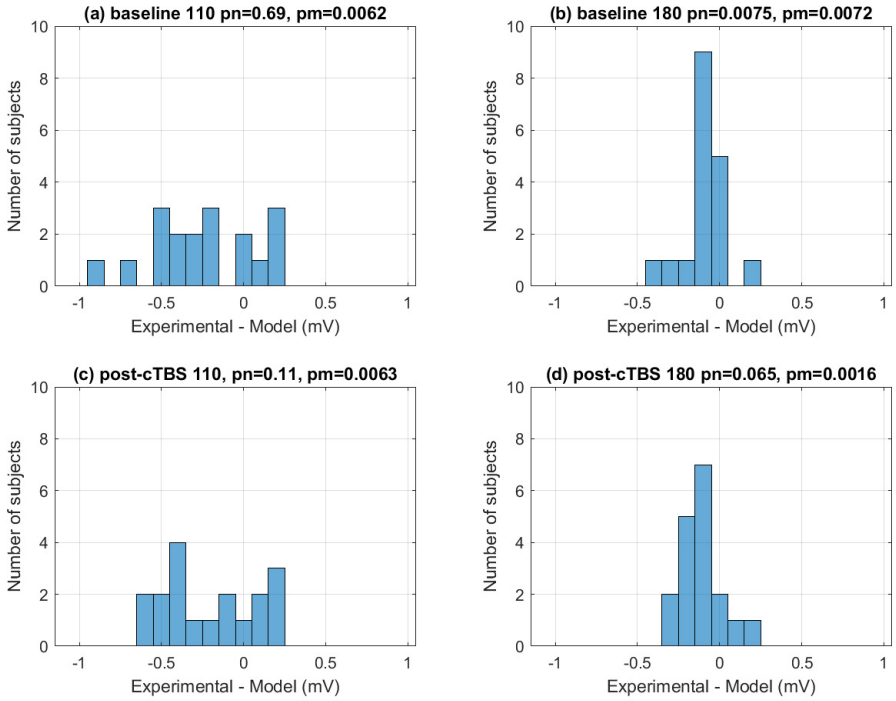

Figure 10: Histograms of the residual MEPs (in millivolts), defined as the experimental MEP minus the modeled MEP, for the cTBS experiments and modeling. (a) Baseline (pre-cTBS), 110% RMT. (b) Baseline, 180% RMT. (c) Post-cTBS, 110%RMT. (d) Post-cTBS, 180% RMT. The p-values for tests of normality (pn) and zero-mean (pm) are shown.

Table 3: Statistical tests on the histograms of the residuals after fitting IO curves to each subject. The table shows test statistics and their p-values. Where the Anderson-Darling test for normality shows a p-value of less than 0.05, the test of whether the mean of the population is zero (t-test) is dubious. Skewness has been tested with the method of Trujillo-Ortiz and Hernandez-Walls (2003).

	iTBS				cTBS			
	baseline		post		baseline		post	
	110%	180%	110%	180%	110%	180%	110%	180%
test statistic								
Anderson-Darling	0.37	0.31	0.41	0.39	0.26	1.03	0.58	0.67
t-test	−4.12	−1.19	−3.68	0.16	−3.13	−3.05	−3.12	−3.76
Skewness	0.72	0.78	1.40	1.76	0.32	1.79	0.26	2.21
p-value for test								
Anderson-Darling	0.41	0.54	0.32	0.35	0.69	0.0075	0.11	0.065
t-test	0.00072	0.25	0.0019	0.88	0.0062	0.0072	0.0063	0.0016
Skewness	0.47	0.44	0.16	0.079	0.75	0.073	0.80	0.027

shows that strong experimental relative response can be related to a change in net excitatory synaptic coupling in the modeling. The changes in w_{ee} from pre- to post stimulation for the various individuals are shown in parts (e) and (f). There is no reduction in w_{ee} as assessed by a paired t-test ($p = 0.065$). The changes in μ from their values pre-stimulation to their values post-stimulation for the various individuals are shown in parts (g) and (h); changes are not statistically significant ($p = 0.092$). Figure 8 shows similar plots for the case of cTBS. Part (e) and (f) show changes in w_{ee}; a paired t-test shows a statistically-significant reduction ($p = 0.035$). Parts (g) and (h) show changes in μ; these are not statistically significant ($p = 0.77$).

4. Discussion

In this work, we asked two questions. First, we asked what phenomonological changes were evident in the IO curves of Goldsworthy et al. (2016). Secondly, we asked whether a biophysical model, specifically that of Wilson et al. (2021) could be used to identify biophysical changes that underly the changes in MEPs.

4.1. Changes in IO curves

First, analysis of the IO curves pre- and post- iTBS and -cTBS shows that there is considerable variation for different individuals. Not only does the MEP amplitude vary considerably, but the rate at which the MEP rises as stimulation amplitude (%RMT) is increased is highly variable, as exemplified in Fig. 5. Changes in IO curves post-iTBS or -cTBS are small for most individuals, and are highly variable depending on the person. This is in agreement with existing literature on variability of TBS results (Gamboa et al., 2010; Hinder et al., 2014; Sasaki et al., 2018; Ozdemir et al., 2021; Capaday, 2021). In particular, there is high variability in MEP around motor threshold. The post-TBS data presented in terms of the response *relative* to baseline, highlights the sensitivity around threshold, and it is important to identify that the two forms of presenting the same data (IO curves as in Fig. 1(a) and (b) and the relative response as in Fig. 1(c) and (d)) lead to different emphases in the analysis.

4.2. Fitting of models

We now address the second question: Can we use a model to identify biophysical changes post-TBS? To do this, we fitted different combinations of three parameters to each person's baseline and post-TBS IO curves: (i) a scaling of the input amplitude and TMS-to-excitatory coupling threshold with a parameter μ, as in Eq. (2), which we have denoted by 'S'; (ii) the

excitatory-to-excitatory synaptic coupling, w_{ee} which we have denoted by 'ee'; and (iii) the excitatory-to-inhibitory synaptic coupling, w_{ie} which we have denoted by 'ie'. We have assessed how each model performs across all subjects as a whole, for the two cases of iTBS and cTBS. Each combination of parameters has been assessed in terms of how well it can model the individual IO curves across the whole population of subjects, using the AIC as described in Eq. (4). The scores for each model are shown in Table 2.

It is clear from these results that no single parameter is sufficient to provide a good fit to the pre- or post-TBS curves. For iTBS, variation in w_{ee} along with μ (i.e. the S+ee model), or w_{ie} along with μ (the S+ie model) are sufficient to describe the baseline IO curves, although S+ee+ie is also a possibility. With cTBS, the S+ee+ie model is most strongly favored. We have therefore picked the S+ee+ie model as our starting point for considering variations in parameters post-TBS, as in Fig. 3(b), second box. Post-TBS, the favored models are S+ee or S+ie for the iTBS case, and S+ee for the cTBS case. This leads us to concentrating on the S+ee case for analysis post stimulation, Fig. 3(b), third box.

The necessity for scaling the input amplitude, 'S' in the models (equivalent to scaling the threshold and width of the TMS-to-excitatory coupling, as in Eq. (2)), is likely to be associated with the large range of TMS thresholds seen across a population of individuals. For example, Goetz et al. (2019) and Capaday (2021) highlight the wide variation in motor thresholds and how the errors in determining motor threshold can result in a large error in measured MEP at intensities close to threshold, as exemplified in Fig. 6.

On a population basis, the S+ee+ie model (pre-TBS) and the S+ee model (post-TBS) fit the IO curves well, as shown in Fig. 7(a) and Fig 8(a) for the cases of iTBS and cTBS respectively. Values of R^2 are all greater than 0.95. We note that the χ^2 values of Table 2 for the S+ee+ie fit to the baseline data are around half of that for the next best fitting models (S+ee or S+ie), showing that the three parameters are needed to produce a good fit. However, post-TBS the χ^2 values for S+ee+ie are of the same order as S+ee and S+ie; in other words the addition of an extra parameter has not made a substantial improvement in fit quality. Figures 7(a) and 9(a) & (c) show, for iTBS, that the model overpredicts MEPs at 110%RMT for both baseline and post-iTBS cases. For the case of cTBS, Figs. 8(a) and 10(a) & (c) show a small overprediction of MEP at both 110%RMT and 180%RMT, although it should also be noted that mean modeled MEP fits the mean experimental MEP better for the cTBS experiments than for the iTBS experiments.

When one looks specifically at relative MEP response following TBS, the situation is complicated further. Experimental results for iTBS show a clear rise in MEPs close to threshold post-stimulation, compared to pre-

stimulation. This is most pronounced at 110%RMT. However, the S+ee model, which gives a favorable AIC score for fitting the IO-curve post-TBS, does not adequately capture this high rise in MEP, as shown in Fig. 7(c). For the cTBS case, the S+ee model is still able to broadly capture the overall depression in MEP across all intensities above threshold, Fig. 8(c). However, below threshold, where MEPs are small, the experimental results show an increase in MEP which has not been captured by the model.

The S+ee+ie fit to the baseline IO curves describes IO curves on an *individual* (rather than population average) basis. Figs. 7(b) and 8(b) for iTBS and cTBS respectively show (for nearly all subjects) a strong correlation between the experimental first principal component values, $\tilde{P}_j$, and the modeled values, P_j, showing that the S+ee+ie model will give an IO curve that gives a similar response as seen experimentally. We emphasize that each IO curve consists of responses at ten intensities, and to fully analyze the situation we will need to consider response for all these ten intensities. The use of the first principal component allows us to describe each IO curve with just one value, facilitating comparison between experiment and modeling across all individuals.

Post-TBS, the change in w_{ee} correlates well with the experimental relative response, on an individual basis, as shown in Fig. 7(d) and Fig. 8(d). This allows us to identify a change in excitatory-to-excitatory weight post-TBS, based on an individual's response curve. However, changes in the best-fit parameters from pre- to post-stimulation are subtle. Fig. 7(e) and (f) shows how w_{ee} has changed for each individual for iTBS, and Fig. 8(e) and (f) shows the same for cTBS. For the cTBS case, there is a small reduction in w_{ee}; for the iTBS case, no statistically significant change is apparent. No changes in the mean values of μ can be identified.

Therefore, although we cannot distinguish changes in parameters on a population basis (e.g. we cannot say that excitatory-to-excitatory weights change on average post-iTBS or post-iTBS), we can say that individuals who exhibit a greater change in response have a greater change in excitatory weight than individuals with less change in response.

4.3. Limitations

This approach has limitations. First, we emphasize that the analysis has been based on a limited range of previously-published experimental data. Specifically, 18 subjects have been used for both the iTBS and cTBS experiments, and IO curves have been recorded at 10 intensities, both before and after TBS (Vallence et al., 2015; Goldsworthy et al., 2016). The cTBS experiments were repeated over three sessions (Vallence et al., 2015). Overall, this is low for modern studies in TBS.

We assume that it is possible to attribute experimentally-measured changes in MEPs to underlying biophysical changes through a model. Given that much of the underlying biophysics is poorly understood (Moezzi et al., 2017; Goetz et al., 2019), for example how a TMS pulse couples to cell populations and the mechanisms of corticospinal activation, such biophysical models will necessarily be limited. Extensive validation of a model will be required in order for there to be real confidence in interpreting fitted values. Direct validation is difficult since it would involve an independent measure of synaptic couplings, which is not feasible except through *in vivo* animal experiments (Barry et al., 2014; Lenz et al., 2016). We note that the neural field model NFTsim, and similar neural field approaches, have been applied successfully to numerous phenomena including anaesthesia, sleep and epilepsy by using parameter values commensurate with the situation, that is, linking underlying biophysical descriptions directly to measured phenomena, usually the electroencephalogram (Robinson et al., 1997; Roberts and Robinson, 2012; Pinotsis et al., 2014; Breakspear, 2017). This gives some confidence that biophysical parameters can be associated with measured outputs. However, the process of MEP formation is more indirect, and this adds a layer of complication to the modeling. The highly nonlinear shape of the IO curve complicates fitting of models and their interpretation in terms of underlying biophysics. A statistical approach to modeling MEPs, including underlying nonlinear processes and noise, is discussed in Goetz et al. (2019). Moreover, Goetz et al. (2022) demonstrated that using simple linear averages of MEPs to quantify response is problematic since it does not adequately capture the underlying processes. Notably, variability in response can be a result of different processes that lead to different statistical distributions.

We also emphasize that the approach taken, using AIC scores as a measure of performance of a model, implicitly will choose one of the candidate models regardless of how good the fits actually are. Thus, while we have focused on S+ee+ie to fit baseline data and S+ee for the post-TBS data, these are not necessary good or the best models. Experimentally, one could test the hypothesis that changes in excitatory circuits, but not inhibitory circuits, explain changes in IO curves post-TBS. Paired-pulse TMS could be used alongside IO curve measurements to measure intracortical facilitation (ICF) and short-interval intracortical inhibition (SICI). The paired-pulse approach would provide an experimental measure of excitatory and inhibitory changes on an individual basis, which could be correlated to the changes predicted by fitting a MEP model to the IO curve.

The MEP model and underlying NFTsim model have many parameters. It is not completely clear which parameters are most relevant for interpreting underlying MEP changes. Wilson et al. (2021) demonstrated that MEPs are

sensitive to several underlying variables. In particular, synaptic couplings between populations have significant affect on MEP amplitudes, while the TMS-to-excitatory population coupling parameters for threshold and width, A and B respectively in Eq. (1) have significant effect on the rate of increase in MEP with increasing stimulation intensity. Moreover, there is considerable experimental and modeling literature that considers variation in synaptic couplings as an underlying cause for measureable changes brain responses (Thickbroom, 2007; Delvendahl et al., 2012; Lenz et al., 2016), and thus synaptic couplings, along with the threshold and width characteristics, are a reasonable choice for fitting to experimental MEP data.

Finally, we comment on the use of RMT as a normalizing feature on IO curves. It is normal practice to identify a RMT based on an individual's response to single pulses of various amplitudes. This is required since different individuals can have very different responses to stimuli. However, presenting IO curves normalized by RMT, without concominant presentation of amplitude data, as is common practice in publications, loses this information and results in an apparent reduction in variability from person-to-person. We suggest that publications of IO data also include absolute amplitude values. Moreover, uncertainties in identifying motor threshold can have a significant effect on the presented curve when normalized by RMT (Goetz et al., 2019). Experimentally, we might be able to assess the impact of threshold identification by assessing model fits with thresholds identified in different ways, such as relative frequency methods and adaptive threshold methods (Groppa et al., 2012). Our work highlights the differences in model interpretation that arise depending on whether one fits models using IO curves or relative responses; in our iTBS modeling the former is reasonably represented (near-lowest AIC value) through the S+ee model, but this cannot capture the significant response near threshold seen in the latter.

5. Conclusions

In this study we have fitted a MEP model (Wilson et al., 2021) to existing experimental data, specifically the input-output response curves measured in the experiments of Goldsworthy et al. (2016). This dataset, which we acknowledge is limited in scope, includes IO curves at ten intensities for 18 subjects, both pre- and post-iTBS and cTBS. Our aim has been to use the model to identify changes in biophysical parameters that occur following iTBS or cTBS. In order to fit the IO curves for populations and individuals well, three parameters have been used: a scaling on input amplitude, equivalent to scaling the threshold and width of the TMS-to-excitatory coupling response, Eq. (2); the excitatory-to-excitatory synaptic coupling; and

the excitatory-to-inhibitory synaptic coupling. We have considered different combinations of changes in these three parameters, meaning that one of these combinations will be 'selected' as the most successful approach regardless of how well it actually does. Changes in these three parameters allow fits both experimental IO data and data presented as relative responses post-TBS, although the fits are better for the former. We emphasize that the manner of presentation of the experimental data, as IO curves or relative responses, makes a difference in terms of analysis and interpretation. For the Goldsworthy et al. (2016) dataset, the model fits give no change in average synaptic couplings or thresholds and widths across a population, but on an individual basis changes in excitatory synaptic coupling do strongly correlate with changes in post-TBS response relative to pre-TBS response.

Author statement

Marcus Wilson: Conceptualization, Methodology, Software, Writing – Original Draft. **Mitchell Goldsworthy:** Investigation, Writing – Review & Editing. **Ann-Maree Vallence:** Investigation, Writing – Review & Editing. **Alex Fornito:** Conceptualization, Writing – Review & Editing. **Nigel Rogasch:** Conceptualization, Methodology, Writing – Original Draft.

Conflict of interest

None of the authors have potential conflicts of interest to be disclosed.

Acknowledgments

NCR is supported by an Australian Research Council DECRA fellowship (DE180100741). MRG is supported by an Australian Research Council DECRA fellowship (DE200100575). AMV is supported by an Australian Research Council DECRA fellowship (DE190100694). AF was supported by the Sylvia and Charles Viertel Charitable Foundation, National Health and Medical Research Council (IDs: 1197431 & 1146292) and the Australian Research Council (DP200103509).

References

Akaike, H.. A new look at the statistical model identification. IEEE Transactions on automatic control 1974;19:716–723.

Barry, M.D., Boddington, L.J., Igelström, K.M., Gray, J.P., Shemmell, J., Tseng, K.Y., Oorschot, D.E., Reynolds, J.N.. Utility of intracerebral theta burst electrical stimulation to attenuate interhemispheric inhibition and to promote motor recovery after cortical injury in an animal model. Experimental Neurology 2014;261:258–266.

Bikson, M., Rahman, A., Datta, A., Fregni, F., Merabet, L.. High-resolution modeling assisted design of customized and individualized transcranial direct current stimulation protocols. Neuromodulation: Technology at the Neural Interface 2012;15(4):306–315.

Breakspear, M.. Dynamic models of large-scale brain activity. Nature Neuroscience 2017;20:340–352.

Brownjohn, P.W., Reynolds, J.N., Matheson, N., Fox, J., Shemmell, J.B.. The effects of individualized theta burst stimulation on the excitability of the human motor system. Brain Stimulation 2014;7(2):260–268.

Capaday, C.. On the variability of motor-evoked potentials: experimental results and mathematical model. Experimental Brain Research 2021;:1–17.

Cooke, S.F., Bliss, T.V.P.. Plasticity in the human central nervous system. Brain 2006;129(7):1659–1673.

Deco, G., Jirsa, V.K., Robinson, P.A., Breakspear, M., Friston, K.. The dynamic brain: from spiking neurons to neural masses and cortical fields. Public Library of Science Computational Biology 2008;4(8):e1000092.

Delvendahl, I., Jung, N.H., Kuhnke, N.G., Ziemann, U., Mall, V.. Plasticity of motor threshold and motor-evoked potential amplitude – a model of intrinsic and synaptic plasticity in human motor cortex? Brain Stimulation 2012;5(4):586–593.

Di Lazzaro, V., Profice, P., Ranieri, F., Capone, F., Dileone, M., Olivero A. Pilato, F.. I-wave origin and modulation. Brain Stimulation 2012;5:512–525.

Esser, S.K., Hill, S.L., Tononi, G.. Modeling the effects of transcranial magnetic stimulation on cortical circuits. Journal of Neurophysiology 2005;94(1):622–639.

Fung, P.K., Haber, A.L., Robinson, P.A.. Neural field theory of plasticity in the cerebral cortex. Journal of Theoretical Biology 2013;318:44–57.

Fung, P.K., Robinson, P.A.. Neural field theory of calcium dependent plasticity with applications to transcranial magnetic stimulation. Journal of Theoretical Biology 2013;324:72–83.

Fung, P.K., Robinson, P.A.. Neural field theory of synaptic metaplasticity with applications to theta burst stimulation. Journal of Theoretical Biology 2014;340:164–176.

Gamboa, O.L., Antal, A., Moliadze, V., Paulus, W.. Simply longer is not better: reversal of theta burst after-effect with prolonged stimulation. Experimental Brain Research 2010;204:181–187.

Goetz, S.M., Alavi, S.M.M., Deng, Z., Peterchev, A.V.. Statistical model of motor-evoked potentials. IEEE Transactions on Neural Systems and Rehabilitation Engineering 2019;27(8):1539–1545.

Goetz, S.M., Howell, B., Wang, B., Li, Z., Sommer, M.A., Peterchev, A.V., Grill, W.M.. Isolating two sources of variability of subcortical stimulation to quantify fluctuations of corticospinal tract excitability. Clinical Neurophysiology 2022;138:134–142.

Goldsworthy, M.R., Vallence, A.M., Hodyl, N.A., Semmler, J.G., Pitcher, J.B., Ridding, M.C.. Probing changes in corticospinal excitability following theta burst stimulation of the human primary motor cortex. Clinical Neurophysiology 2016;127:740–747.

Groppa, S., Oliviero, A., Eisen, A., Quartarone, A., Cohen, L., Mall, V., Kaelin-Lang, A., Mima, T., Rossi, S., Thickbroom, G., Rossini, P., Ziemann, U., Valls-Solé, J., Siebner, H.. A practical guide to diagnostic transcranial magnetic stimulation: Report of an ifcn committee. Clinical Neurophysiology 2012;123(5):858–882.

Hallett, M.. Transcranial magnetic stimulation and the human brain. Nature 2000;406:147–150.

Hallett, M.. Transcranial magnetic stimulation: A primer. Neuron 2007;55:187–199.

Hinder, M.R., Goss, E.L., Fujiyama, H., Canty, A.J., Garry, M.I., Rodger, J., Summers, J.J.. Inter- and intra-individual variability following intermittent theta burst stimulation: Implications for rehabilitation and recovery. Brain Stimulation 2014;7(3):365–371.

Huang, Y.Z., Edwards, M.J., Rounis, E., Bhatia, K.P., Rothwell, J.. Theta burst stimulation of the human motor cortex. Neuron 2005;45:201–206.

Ilic, T.V., Meintzschel, F., Cleff, U., Ruge, D., Kessler, K.R., Ziemann, U.. Short-interval paired-pulse inhibition and facilitation of human motor cortex: the dimension of stimulus intensity. Journal of Physiology London 2002;545:153–167.

Klimesch, W., Sauseng, P., Gerloff, C.. Enhancing cognitive performance with repetitive transcranial magnetic stimulation at human individual alpha frequency. European Journal of Neuroscience 2003;17(5):1129–1133.

Kujirai, T., Caramia, M.D., Rothwell, J.C., Day, B.L., Thompson, P.D., Ferbert, A., Wroe, S., Asselman, P., Marsden, C.D.. Corticocortical inhibition in human motor cortex. Journal of Physiology 1993;471:501–519.

Lefaucheur, J.P., André-Obadia, N., Antal, A., Ayache, S.S., Baeken, C., Benninger, D.H., Cantello, R.M., Cincotta, M., de Carvalho, M., De Ridder, D., et al. Evidence-based guidelines on the therapeutic use of repetitive transcranial magnetic stimulation (rTMS). Clinical Neurophysiology 2014;125(11):2150–2206.

Lenz, M., Galanis, C., Müller-Dahlhaus, F., Opitz, A., Wieranga, C.J., Szabó, G., Ziemann, U., Deller, T., Funke, K., Vlachos, A.. Repetitive magnetic stimulation induces plasticity of inhibitory synapses. Nature Communications 2016;7:10020.

Matheson, N.A., Shemmell, J.B.H., De Ridder, D., Reynolds, J.N.J.. Understanding the effects of repetitive transcranial magnetic stimulation on neuronal circuits. Frontiers in Neural Circuits 2016;10:67.

Moezzi, B., Schaworonkow, N., Plogmacher, L., Goldsworthy, M.R., Hordacre, B., McDonnell, M.D., Iannella, N., Ridding, M.C., Triesch, J.. Simulation of electromyographic recordings following transcranial magnetic stimulation. Journal of Neurophysiology 2017;120:2532–2541.

Ozdemir, R.A., Boucher, P., Fried, P.J., Momi, D., Jannati, A., Pascual-Leone, A., Santarnecchi, E., Shafi, M.M.. Reproducibility of cortical response modulation induced by intermittent and continuous theta-burst stimulation of the human motor cortex. Brain Stimulation 2021;14(4):949–964.

Pascual-Leone, A., Walsh, V., Rothwell, J.. Transcranial magnetic stimulation in cognitive neuroscience–virtual lesion, chronometry, and functional connectivity. Current Opinion in Neurobiology 2000;10(2):232–237.

Pinotsis, D., Robinson, P., beim Graben, P., Friston, K.. Neural masses and fields: modeling the dynamics of brain activity. Frontiers in Computational Neuroscience 2014;8:149.

Roberts, J.A., Robinson, P.A.. Corticothalamic dynamics: Structure of parameter space, spectra, instabilities, and reduced model. Physical Review E 2012;85:011910.

Robinson, P., Rennie, C., Rowe, D., O'Connor, S.. Estimation of multiscale neurophysiologic parameters by electroencephalographic means. Human Brain Mapping 2004;23(1):53–72.

Robinson, P.A., Rennie, C.J., Wright, J.J.. Propagation and stability of waves of electrical activity in the cerebral cortex. Physical Review E 1997;56:826–840.

Rogasch, N.C., Fitzgerald, P.B.. Assessing cortical network properties using TMS-EEG. Human Brain Mapping 2013;34(7):1652–1669.

Rusu, C.V., Murakami, M., Ziemann, U., Triesch, J.. A model of TMS-induced I-waves in motor cortex. Brain Stimulation 2014;7:401–414.

Sanz-Leon, P., Robinson, P.A., Knock, S.A., Drysdale, P.D., Abeysuriya, R.G., Fung, P.K., Rennie, C., Zhao, X.. NFTsim: Theory and simulation of multiscale neural field dynamics. PLoS Computational Biology 2017;14:e1006387.

Sasaki, T., Kodama, S., Togashi, N., Shirota, Y., Sugiyama, Y., Tokushige, S.i., Inomata-Terada, S., Terao, Y., Ugawa, Y., Hamada, M.. The intensity of continuous theta burst stimulation, but not the waveform used to elicit motor evoked potentials, influences its outcome in the human motor cortex. Brain Stimulation 2018;11(2):400–410.

Saturnino, G.B., Puonti, O., Nielsen, J.D., Antonenko, D., Madsen, K.H., Thielscher, A.. SimNIBS 2.1: a comprehensive pipeline for individualized electric field modelling for transcranial brain stimulation. In: Makarov, S., Horner, M., Noetscher, G., editors. Brain and Human Body Modeling. Cham, Switzerland: Springer Open; 2019. p. 3–25.

Sorkhabi, M.M., Wendt, K., Wilson, M.T., Denison, T.. Numerical modeling of plasticity induced by quadri-pulse stimulation. IEEE Access 2021;9:26484–26490.

Tang, A.D., Hong, I., Boddington, L.J., Garrett, A.R., Etherington, S., Reynolds, J.N.J.. Low intensity repetitive magnetic stimulation lowers action potential threshold and increases spike firing in layer 5 pyramidal neurons in vitro. Neuroscience 2016;335:64–71.

Thickbroom, G.W.. Transcranial magnetic stimulation and synaptic plasticity: experimental framework and human models. Experimental Brain Research 2007;180:583–593.

Traub, R.D., Buhl, E.H., Gloveli, T., Whittington, M.A.. Fast rhythmic bursting can be induced in layer 2/3 cortical neurons by enhancing persistent Na^+ conductance or by blocking BK channels. Journal of Neurophysiology 2003;89(2):909–921.

Trujillo-Ortiz, A., Hernandez-Walls, R.. skekurtest: Hypotheses test concerning skewness and kurtosis. a MATLAB file. `http://www.mathworks.com/matlabcentral/fileexchange/loadFile.do?objectId=3953&objectType=FILE`; 2003. Accessed: 1 October 2022.

Vallence, A.M., Goldsworthy, M., Hodyl, N., Semmler, J., Pitcher, J., Ridding, M.. Inter- and intra-subject variability of motor cortex plasticity following continuous theta-burst stimulation. Neuroscience 2015;304:266–278.

Valls-Solé, J., Pascual-Leone, A., Wassermann, E.M., Hallett, M.. Human motor evoked responses to paired transcranial magnetic stimuli. Electroencephalography and Clinical Neurophysiology/Evoked Potentials Section 1992;85(6):355–364.

Wilson, M.T., Fulcher, B.D., Fung, P.K., Robinson, P.A., Fornito, A., Rogasch, N.C.. Biophysical modeling of neural plasticity induced by transcranial magnetic stimulation. Clinical Neurophysiology 2018;129:1230–1241.

Wilson, M.T., Fung, P.K., Robinson, P.A., Shemmell, J., Reynolds, J.N.J.. Calcium dependent plasticity applied to repetitive transcranial magnetic stimulation with a neural field model. Journal of Computational Neuroscience 2016;49:107–125.

Wilson, M.T., Goodwin, D.P., Brownjohn, P.W., Shemmell, J., Reynolds, J.N.J.. Numerical modelling of plasticity induced by transcranial magnetic stimulation. Journal of Computational Neuroscience 2014;36:499–514.

Wilson, M.T., Moezzi, B., Rogasch, N.C.. Modeling motor-evoked potentials from neural field simulations of transcranial magnetic stimulation. Clinical Neurophysiology 2021;132(2):412–428.

Ziemann, U., Paulus, W., Nitsche, M.A., Pascual-Leone, A., Byblow, W.D., Berardelli, A., Siebner, H.R., Classen, J., Cohen, L.G., Rothwell, J.C.. Consensus: motor cortex plasticity protocols. Brain Stimulation 2008;1(3):164–182.

Ziemann, U., Rothwell, J.C., Ridding, M.C.. Interaction between intracortical inhibition and facilitation in human motor cortex. The Journal of physiology 1996;496(3):873–881.